Chemical Science

EDGE ARTICLE

View Article Online
View Journal | View Issue

Cite this: *Chem. Sci.*, 2014, **5**, 2536

Conformational control of anticancer activity: the application of arene-linked dinuclear ruthenium(II) organometallics†

Benjamin S. Murray,* Laure Menin, Rosario Scopelliti and Paul J. Dyson*

Dinuclear metal complexes have emerged as a promising class of biologically active compounds which possess unique anticancer activity. Here, we describe a novel series of arene-linked dinuclear organometallic Ru(II) complexes, where the relative conformation of the ruthenium centres is controlled by the stereochemical configuration of 1,2-diphenylethylenediamine linker moieties, as confirmed by X-ray crystallography. The reactivity and cytotoxicity of these compounds is compared to flexible dinuclear and mononuclear analogues, demonstrating in all cases the complexes can undergo aquation, coordinate to typical biological donor ligands and importantly, in the case of dinuclear analogues, crosslink oligonucleotide and peptide sequences. Differences in the conformation of the isomeric dinuclear compounds lead to significantly different levels of cytotoxicity against A2780, A2780cisR and HEK-293 cell lines; isomers with a closed conformation are significantly more cytotoxic than isomers with a more open conformation and they are also significantly less susceptible to acquired resistance mechanisms operating in the A2780cisR cell line. These rigid dinuclear compounds possess markedly increased cytotoxicity relative to the non-cytotoxic mononuclear analogues that does not appear to be related to differences in complex lipophilicity or cellular uptake, which, in general, remain similar in magnitude across the series. Thus, the molecular conformation of such dinuclear species may be crucial in determining the nature of the adducts formed on coordination to biological targets in a cellular environment, and opens up a novel route toward the development of more active metal-based anticancer agents.

Received 11th January 2014
Accepted 24th March 2014

DOI: 10.1039/c4sc00116h

www.rsc.org/chemicalscience

Introduction

Metal-based compounds offer considerable potential in medicinal chemistry where the careful choice of metal may afford compounds possessing geometrical, coordination and potentially catalytic properties not accessible through purely organic molecules. As a result, the judicious combination of a metal ion and associated ligands may result in complexes capable of unique biological activity. In the context of developing metal-based drugs for the treatment of cancer, considerable effort has been directed toward the development of novel platinum complexes,[1] stemming from the clinical success of cisplatin (and subsequent derivatives).

Apart from the platinum family of metallodrugs several other metals have been utilised in the development and identification of further classes of compounds that exhibit favourable medicinal attributes. Of these, ruthenium-based organometallic compounds constitute a rapidly developing field that continues to yield complexes exhibiting diverse biological activity.[2] Prominent examples include the $[Ru(\eta^6\text{-arene})(en)Cl]^+$ family of organometallics that has yielded compounds with a comparable cytotoxicity to that of cisplatin in certain cell lines.[3] Structurally related compounds based on the $[Ru(\eta^6\text{-arene})(L)Cl]^+$ scaffold, with organic ligands (L) chosen because of their various biological activities, also exhibited significant antiproliferative activity against a range of cancer cell lines.[4–6] An alternative strategy, based on the development of kinetically inert ruthenium half-sandwich complexes as potent inhibitors of protein kinases, has also led to complexes exhibiting high cytotoxicity against the HCT-116 cell line.[7] Ru(II)–arene complexes have also been incorporated into multinuclear systems and assessed for their anticancer activity. These have included metalla-cycles,[8–12] metalla-cages[13–15] and dendrimer-based systems.[16] Of particular interest to us are the $[Ru(\eta^6\text{-arene})Cl_2(PTA)]$ (RAPTA) series of organometallic ruthenium(II) compounds which display selective activity on metastatic tumours *in vivo*.[17,18] Recent work

Institut des Sciences et Ingénierie Chimiques, Ecole Polytechnique Fédérale de Lausanne (EPFL), CH-1015, Lausanne, Switzerland. E-mail: paul.dyson@epfl.ch; Fax: +41 (0)21 693 97 80; Tel: +41 (0)21 693 98 54

† Electronic supplementary information (ESI) available: Experimental procedures for all novel compounds and copies of nuclear magnetic resonance spectra, X-ray diffraction parameters, HPLC chromatograms for arene ligands of **5a** and **6a**, UV-vis spectra and selected mass spectra. CCDC 978401–978404. For ESI and crystallographic data in CIF or other electronic format see DOI: 10.1039/c4sc00116h

observed that proteins are a major intracellular target of the RAPTA compounds,[19] including the histone proteins of the nucleosome core particle. Structural studies also show that RAPTA-C binds to the protein component of the nucleosome core particle in preference to the nucleic acid component.[20] In addition, subcellular localisation of RAPTA-T in A2780 and A2780cisR cells revealed higher metal to protein ratios in the particulate fraction (including the mitochondria) relative to the cytosol and nuclear fractions.[19] Further accounts have described selective binding of RAPTA-C within protein mixtures[21] and also potent enzyme inhibition by RAPTA compounds.[22,23] These studies offer an insight into the potential of the RAPTA compounds to exert their biological activity through protein interactions rather than DNA damaging mechanisms characteristic of the vast majority of platinum metallodrugs reported so far. We reasoned that dinuclear analogues of the RAPTA series may exhibit a different spectrum of biological activity compared to mononuclear RAPTA derivatives, potentially retaining the propensity of the mononuclear RAPTA compounds to bind proteins while acting *via* crosslinking of target biomolecules through long-range interactions rather than short range interactions typical of mononuclear species. In the field of platinum metallodrugs the formation of dinuclear analogues has been a successful route toward the development of compounds capable of unique binding modes and interactions with DNA.[24] This approach has led to compounds of increased potency compared to established mononuclear platinum compounds which retain high activity in cell lines resistant to cisplatin.[25,26] In contrast, dinuclear organometallic ruthenium(II) arene compounds are underexplored.[27] In the most comprehensive of these studies to date a series of dinuclear ruthenium compounds linked *via* maltol-derived ligands were investigated.[28–30] The cytotoxicity of these compounds was found to be tuned by modification of the chain length of the alkyl component of the linker ligand, with cytotoxicity correlating well to the experimentally determined lipophilicity of the resulting complexes.[28] Of notable interest is the observation that not only could these complexes crosslink two DNA duplexes but also that DNA–protein crosslinks could be formed, potentially a novel mode of action for such complexes.[30]

We hypothesised that the use of linker ligands rigid enough to fix the relative orientation of the metal centres in a dinuclear RAPTA complex would allow access to a series of isomeric structures of differing conformation. Such complexes would allow an assessment of the effect of conformation on biological activity to be probed, including the manner in which isomeric complexes of different conformation interact with potential target biomolecules.

Here we report the synthesis, binding studies with potential biological targets and *in vitro* biological evaluation of a series of dinuclear Ru(II)–arene compounds, where the conformation of the RAPTA units relative to each other is controlled by the stereochemical configuration of a 1,2-diphenylethylenediamine (DPEN) linker molecule. Compounds with a linking group possessing either an (*R*,*R*)- or (*S*,*S*)-configuration exhibit a more 'closed' conformation whereas those with a (*R*,*S*)-configuration possess an open conformation not dissimilar to that of a complex linked *via* a flexible linker (Fig. 1). Such conformational control could significantly influence the interactions of each complex with biomolecular targets, ultimately yielding a different range of adducts, and potentially controlling the cytotoxicity and selectivity.

In addition to the rigid dinuclear complexes described above a further dinuclear complex, linked together using the flexible ethylene diamine analogue, and a mononuclear analogue are also reported. Our approach was to develop dinuclear Ru(II)–arene compounds linked together through the arene ligand in order to retain the core coordination environment around ruthenium as in the original RAPTA series to avoid significantly perturbing the coordination mode of these dinuclear complexes with potential biological targets.

Results and discussion

Synthesis and characterisation

The synthesis of the ruthenium dimers, and the mononuclear analogue, proceeded *via* amide-forming reactions between the common intermediate complex, **1**, bearing a carboxylic acid substituent on the arene ligand, and the selected amines (Scheme 1). Complex **1** includes a single chelating oxalato-moiety as a protecting group in order to suppress undesired reactions with the ruthenium centre during amide bond formation. Reactions between **1** and the desired amines were performed utilising the coupling agent *O*-(benzotriazol-1-yl)-*N*,*N*,*N*′,*N*′-tetramethyluronium tetrafluoroborate (TBTU) with *N*,*N*-diisopropylethylamine (DIPEA) in DMF, to either yield **3a** and **4a** as DMF-insoluble yellow powders that were isolated by filtration, or monomer analogue **2a** and dinuclear compounds **5a** and **6a** as crude yellow powders following precipitation with acetone. All compounds were further purified by recrystallisation until analytically pure (see ESI†). Each oxalato-protected ruthenium complex was successfully converted to its chlorido-analogue by dissolution in an anhydrous solution of HCl in methanol – the yellow solutions immediately turned red in colour followed by precipitation of the desired dinuclear compounds **3b–6b** as their HCl salts, or in the case of monomer analogue **2b** the product was obtained by precipitation with diethyl ether. All compounds (**1–6b**) are water soluble; the oxalato-protected compounds (**2a–6a**) possess low solubility in DMSO and other organic solvents. All compounds were characterised by ^{1}H, ^{31}P and ^{13}C NMR, high-resolution mass spectrometry and elemental analysis (see ESI†).

The molecular structures of **1**, **2a**, **4a**, **5a** and **6a** (Fig. 2 and S1†) were confirmed by single crystal X-ray crystallography on

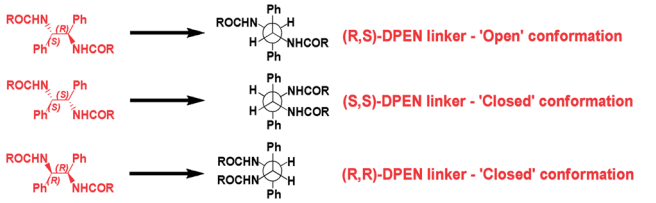

Fig. 1 Newman projections of predicted conformations of dinuclear complexes **4a–6a** and **4b–6b** based on ligand steric demand.

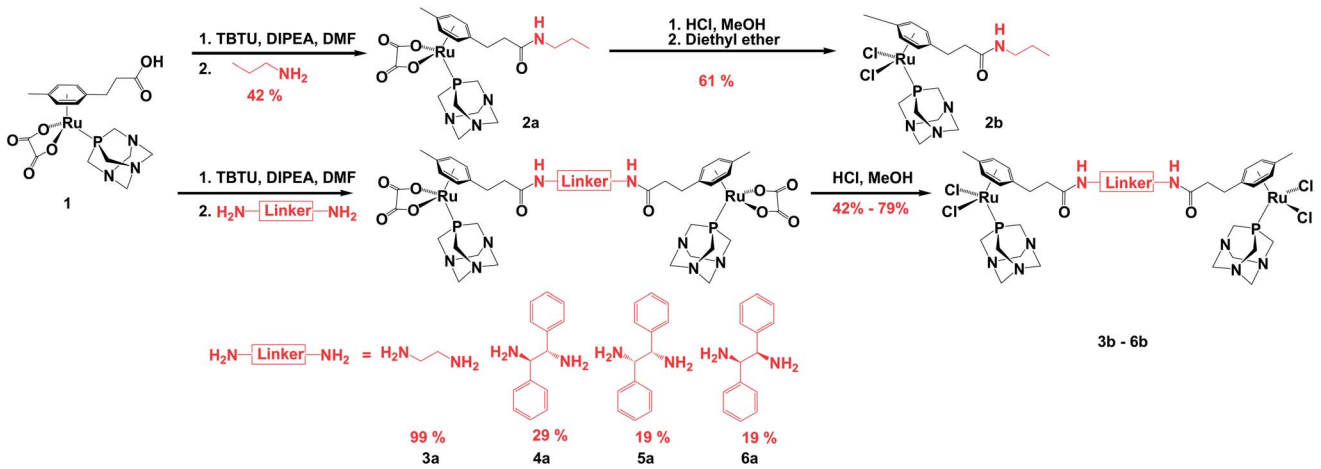

Scheme 1 Synthesis and numbering scheme of the mononuclear oxalato-complex **2a**, dinuclear oxalato-complexes **3a–6a** and chlorido-analogues **2b–6b**.

crystals grown *via* the slow diffusion of diethyl ether into a methanolic solution of the complex (**2a**), or the slow diffusion of acetone into a solution of the complex in H_2O and acetone (**1**, **4a**, **5a** and **6a**). In each case the coordination environment around the central ruthenium ions is similar, adopting the characteristic "piano-stool" configuration. Structural data confirms the stereoisomeric complexes, **4a**, **5a** and **6a**, occupy conformations predicted by the Newman projections of the DPEN linkers (Fig. 1). For the enantiomeric complexes **5a** and **6a** linked by (1*S*,2*S*)-DPEN or (1*R*,2*R*)-DPEN respectively, the structures are of a concave conformation with the *trans*-geometry of the phenyl rings of the linker backbone forcing the two RAPTA units into positions adjacent to one another.‡ In contrast, the conformation of the diastereomeric complex **4a** linked by (1*R*,2*S*)-DPEN is found to be more linear with the two RAPTA substituents being related through a centre of inversion.

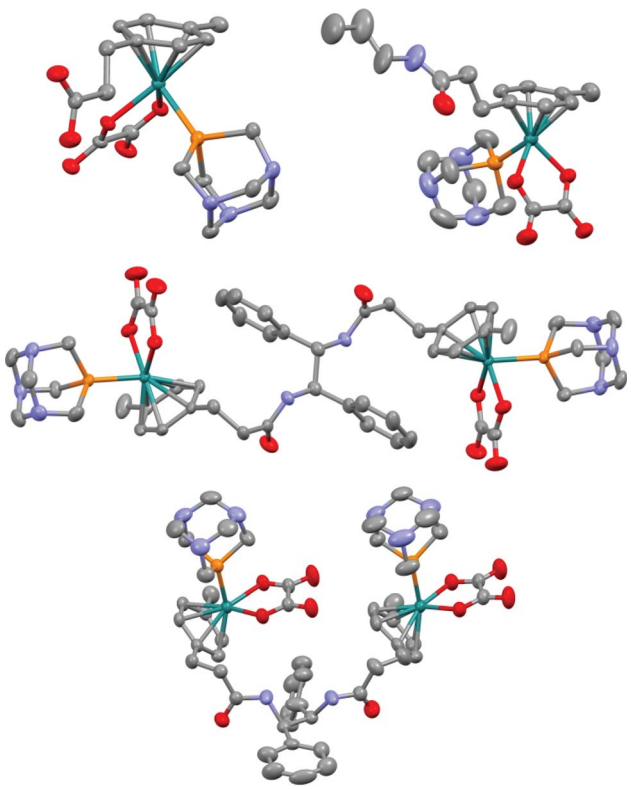

Fig. 2 Molecular structures of **1** (top left), **2a** (top right), **4a** (middle) and **5a**/**6a** (bottom). Hydrogen atoms have been omitted for clarity. Atoms are colour coded: ruthenium – cyan, phosphorus – orange, oxygen – red, nitrogen – purple, carbon – grey. See ESI† for figures of the compounds including atom labels.

^{1}H-NMR spectra of the complexes in D_2O shows that the central linker significantly influences molecular conformation. The spectrum of **3a** (Fig. S30†), in which the RAPTA-units are linked through a flexible ethylene diamine moiety, is relatively simple. Both sets of methylene protons and arene protons manifest as a single set of resonances. In contrast, the spectra of dinuclear complexes constructed with the stereoisomeric 1,2-diphenylethylenediamine linking groups are more complex (Fig. 3), the form of each being dependent on the stereochemical configuration of the linker used. The ^{1}H NMR spectra of the enantiomeric complexes **5a** and **6a** are identical and possess four sets of Ru-coordinated arene resonances which are slightly shielded relative to equivalent resonances observed in the spectra of **1–3a**. The methylene protons give rise to a complex set of resonances between 2.4–2.6 ppm whereas resonances corresponding to the aromatic protons of the linker consist of two peaks between 7.1–7.3 ppm. For the diastereomeric complex, **4a**, two of the four Ru-coordinated arene resonances overlap, with all arene resonances having a different chemical shift compared to those of **5a** and **6a**. Interestingly, one of the arene resonances of **4a** (5.08 ppm) is significantly more shielded relative to the other arene resonances. In addition, the resonance set corresponding to the methylene protons is more shielded and occurs between 2.16–2.33 ppm. These observations correlate well with the observation in the X-ray structure of **4a** that the corresponding protons are shown to reside above the plane of the linker phenyl groups – a magnetic environment which would provide shielding from the applied magnetic field.

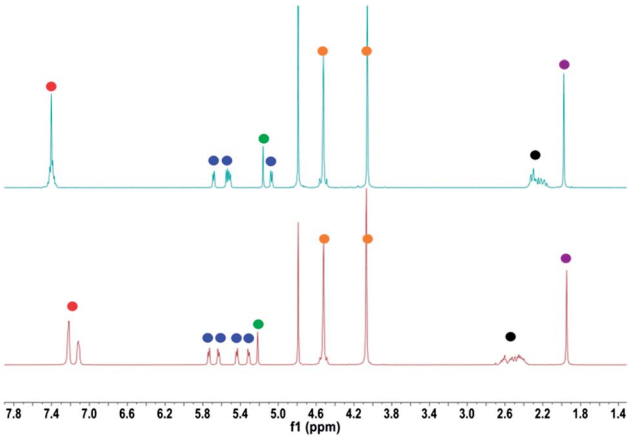

Fig. 3 ^{1}H NMR spectra of **4a** (top) and **5a** (bottom) (D_2O, 400 MHz, 298 K, 10 mM). Resonances are identified with coloured circles: linker phenyl – red, Ru arene – blue, C*H* – green, PTA – orange, CH_2 – black and CH_3 – purple.

Furthermore, in the spectrum of **4a** the linker phenyl protons give rise to a single resonance at 7.4 ppm. The increased complexity in the spectra of **4a–6a** relative to the spectrum of **3a** reflects the increased central rigidity present in the former complexes due to the DPEN linkers. In addition, the shielding observed in the spectrum of **4a** provides direct evidence that the conformation observed in the solid state is also preserved in aqueous solution.

Aquation and stability studies

Many metal complexes, including cisplatin and several families of organometallic ruthenium complexes, are activated on cellular internalization (low [Cl^-]) by aquation of labile metal–chlorido bonds, the aquated species being significantly more labile toward donor groups of biological targets.[31] Early work[17] with a prototypical example of the RAPTA series, RAPTA-C, revealed that upon dissolution in pure water or 4 mM NaCl solution the complex rapidly undergoes exchange of both chlorido ligands for aqua ligands. In 100 mM saline solution this process is completely suppressed.

Oxalato- and chlorido-containing ruthenium compounds synthesised in this work were assessed for their stability and reactivity in phosphate buffer (10 mM) at pH 7.2 in the presence of either 5 mM or 100 mM NaCl at 298 K. The UV-vis spectra of the chlorido analogues **2b–5b** immediately change upon dissolution in phosphate buffer (10 mM) containing NaCl (5 mM), indicative of a change in coordination environment at the Ru centre. The half-lifes of the chlorido complexes (**2b–5b**) were estimated from the change in absorbance with time (see Fig. S5–S9†). In phosphate buffer **3b** possessed the shortest half-life (8.5 min) followed by **2b** (10.5 min), **4b** (13.6 min) then **5b** (17.3 min), the more closed structure of the latter compound presumably slows the aquation process for this complex. For comparison, under these conditions RAPTA-C has a half-life shorter than all compounds described here (6.8 min). These results indicate that although the different structures and conformations of compounds **2b–5b** affect the kinetics of ligand exchange at ruthenium, the 'active' aqua species of each complex may be readily formed on dissolution in low [Cl^-] aqueous solution. In the presence of elevated NaCl concentrations (100 mM) no aquation of these compounds was observed, in accordance with previous results.[17] The oxalato-protected compounds **2a–5a** were also examined by ^{31}P NMR spectroscopy in the presence of HEPES–phosphate buffer (5 mM or 100 mM NaCl), and in the presence of BSA, CT-DNA and glutathione. In each case the appearance of no new ^{31}P-NMR signals were observed over a period of 72 h at 310 K, demonstrating that the oxalato complexes are inert towards aquation or ligand exchange under ambient conditions on the timescale of the experiment. In contrast, on incubation of **2a–5a** in RPMI or DMEM media used for cell culture it was found that a new resonance at −32.4 ppm gradually appears in the ^{31}P NMR spectra over 48 h, with incubation of the complexes in DMEM resulting in the largest transformation (Fig. S10–S16†). The new resonance at −32.4 ppm may be attributed to the exchange of the oxalato ligand for a carbonato ligand as sodium bicarbonate is present in the RPMI and DMEM media used at concentrations of 23.8 mM and 44.0 mM respectively. Subsequent experiments involving the incubation of **2a** with NH_4CO_3H (23.8 mM) in phosphate buffer (pH 7.4, 50 mM) confirmed this hypothesis, as the ^{31}P NMR spectrum after 24 h exhibits the same transformation as the spectra recorded in RPMI/DMEM. The oxalato-protected complexes **2a–6a** are stable toward aquation and inert in the presence of typical biological ligands, whereas media containing bicarbonate at concentration levels typically found in biological systems (10–30 mM), results in the gradual exchange of the oxalato ligand for a carbonato ligand, providing a possible route toward the intracellular activation of the oxalato-protected compounds.

Amino acid and nucleotide binding studies

In order to assess the ability of the complexes to coordinate to and crosslink biological targets, binding studies were performed with guanosine 5′-monophosphate, L-histidine and a range of model oligonucleotides and peptides.

To establish whether each ruthenium ion of the dinuclear compounds **3b–6b** could coordinate simultaneously to target ligands, binding studies were performed initially with guanosine 5′-monophosphate and L-histidine – both being good ligands for RAPTA-type compounds as constituents of DNA or proteins, respectively.[20,32] For each dinuclear complex **3b–6b**, following incubation in the presence of 2 equivalents of 5′-GMP (72 h, 310 K, pH 4.5 unbuffered), electrospray ionization mass spectrometric analysis revealed the presence of a range of 2 : 1 and 1 : 1 5′-GMP–metal complex adducts. Interestingly, for the complexes with the closed conformation, **5b** and **6b**, and the flexible ethylene diamine linker, **3b**, these adducts include examples where all four labile chlorido ligands are lost and replaced with a single 5′-GMP molecule – indicating both ruthenium centres are bridged *via* coordination to the same 5′-GMP ligand. ^{1}H and ^{31}P NMR spectroscopy indicated the most likely coordination sites are N7 and phosphate oxygen (see

below). For the more open complex, **4b**, the conformation of which is expected to be less favourable for intramolecular bridging coordination to occur, the corresponding peaks in the mass spectrum are of a relatively low intensity, the peaks corresponding to 2 : 1 5′-GMP–metal complex adducts are of higher relative intensity (Fig. S17†). Studies with the monomer analogue **2b** reveal the formation of only 1 : 1 5′-GMP–metal complex adducts, even in the presence of 2 equivalents 5′-GMP. For incubations of dinuclear compounds **3b–5b** with 2 equivalents of 5′-GMP at pH 7.5 (310 K, 60 mM ammonium acetate) only 1 : 1 adducts were detected. Adducts include examples where all four chlorido ligands are replaced by a single 5′-GMP ligand, alongside similar adducts also containing a coordinated acetate ligand. It is likely that at pH 7.5 the deprotonation of the 5′-GMP phosphate (pK_a of 6.49 reported for PO_3H of 5′-GMP[33]) facilitates the formation of intramolecularly bridged 1 : 1 adducts in preference to the formation of 2 : 1 5′-GMP–metal complex adducts. Complementary binding studies between 5′-GMP and **3b** were also monitored by ^{1}H and ^{31}P NMR spectroscopy over 24 h (pD = 7.5, 200 mM HEPES buffer, 310 K) (Fig. S18†). Spectra are complex due to the formation of diastereoisomeric adducts upon coordination with 5′-GMP. Multiple new 5′-GMP H8 resonances in the region 8.00–8.85 ppm were identified by ^{1}H NMR spectroscopy corresponding to adducts involving coordination of N7 of 5′-GMP to the ruthenium ion. Concurrent analysis with ^{31}P NMR spectroscopy revealed the appearance of new 5′-GMP resonances (−2.90 to 8.45 ppm) indicative of phosphate coordination to the ruthenium ion alongside N7 coordination. This data complements the observation of intramolecular crosslinking of these dinuclear RAPTA analogues by 5′-GMP as observed in the mass spectrometric studies. A further distinctive proton resonance set, centred at 7.05 ppm, also gradually appeared in the aromatic region of the ^{1}H NMR spectra. This was deduced to be due to formation of the free arene ligand, indicating that upon coordination of 5′-GMP to **3b**, potentially through both phosphate and N7 coordination, the arene ligand is lost from the adduct. In addition, the colour of the solution changed from yellow to black over the 24 h incubation period indicative of complex decomposition. Similar 5′-GMP–Ru adduct(s) were not identified during the mass spectrometric studies although the free arene ligand was detected by ESI-MS in the incubations performed at pH 7.5. The loss of the arene ligand is not unprecedented with similar loss of the arene ligand being reported previously in binding studies of RAPTA-C with a 14-*mer* oligonucleotide.[34]

Binding experiments were also performed with 2 equivalents of L-histidine at pH 7.1 and monitored by ^{1}H and ^{31}P NMR spectroscopy and ESI-MS. As with 5′-GMP, ESI-MS revealed the formation of a range of 1 : 1 adducts between L-histidine and dinuclear compounds **3b–6b**. Bridging of L-histidine between the two ruthenium ions is observed for all the dinuclear compounds; characterised by peaks corresponding to the loss of all four chlorido ligands in exchange for a single histidine, although the intensity of these peaks are relatively low compared to the intensity of other 1 : 1 adduct peaks (Fig. S19†). Peaks corresponding to 2 : 1 L-histidine–metal complex adducts are also observed in all the spectra of the dinuclear compounds, but are of low relative intensity (<15%). For the mononuclear analogue **2b**, in the presence of 2 equivalents of L-histidine, only peaks corresponding to 1 : 1 adducts are observed. ^{1}H NMR spectroscopy indicates that loss of the arene does not take place during the 24 h incubation, and, unlike the 5′-GMP incubation, the colour of the solution remains yellow.

As these small-molecule binding experiments confirm all dinuclear complexes **3b–6b** readily coordinate to appropriate donor ligands simultaneously through both ruthenium atoms, binding studies were expanded to include a short model peptide sequence and a single-stranded 13-*mer* oligonucleotide.

Oligonucleotide and peptide binding studies

Oligonucleotide binding studies were performed on the 13-*mer* sequence 5′-ATACATCGTACAT-3′ in unbuffered aqueous solutions (72 h, 310 K, pH = 4.5, 0.2 mM complex and 2 eq. oligonucleotide). The reaction mixture was then diluted and directly analysed using ESI-MS in negative ionization mode. In higher mass regions of the spectra peaks attributable to 1 : 1 oligonucleotide–metal complex adducts are observed in which the metal complexes have lost their chlorido ligands. No higher order adducts were detected. However, the predominant species in these spectra correspond to oligonucleotide–metal complex adducts where the arene ligand is lost leaving the Ru–PTA fragment coordinated to the oligonucleotide. These results correlate with the NMR binding studies of 5′-GMP with **3b** where loss of the arene ligand was observed.

Peptide binding studies utilised a fragment of amyloid β-protein (residues 1–16, H-Asp-Ala-Glu-Phe-Arg-His-Asp-Ser-Gly-Tyr-Glu-Val-His-His-Gln-Lys-OH). This 16-*mer* contains three histidine residues as well as one lysine and two glutamate residues – all of which have been observed to coordinate to RAPTA compounds in crystallographic studies.[20] Incubations were performed in unbuffered aqueous solutions (72 h, 310 K) in a 1 : 1 peptide–metal complex ratio. Using ESI-MS in all cases a range of 1 : 1 adducts were observed with no 2 : 1 or higher order complex–peptide or peptide–complex adducts detected. As with the small-molecule binding studies, 1 : 1 dinuclear metal complex–peptide adducts are detected where all four labile chlorido ligands are lost (and, in some cases, loss of PTA ligands is also observed) and substituted by a single peptide. The loss of two or three ligands at each Ru centre implies that each metal of the dinuclear compounds must be coordinated to one or more amino acid residues of the peptide. It is likely that crosslinked species where each metal centre is bound to a different amino acid residue form a proportion of these 1 : 1 adducts. ESI mass spectra of peptide adducts of **4b**, **5b** and **6b** reveals a similar peak distribution (Fig. S20†). To probe the nature of the binding within these 1 : 1 adducts electron-transfer dissociation (ETD) fragmentation studies were performed on selected ions.

Electron-transfer dissociation (ETD) fragmentation and ion mobility-mass spectrometry (IM-MS) studies

ETD fragmentation of peptides is an established technique used to randomly fragment the N–C_α bonds of a peptide backbone. This technique often preserves post-translational modifications of the peptide side chains, such as phosphorylation and glycosylation, allowing their identification and localisation in a peptide sequence to be determined.[35] More recently, this technique has been used to identify drug metallation sites in peptide[36] and protein samples.[37] We used ETD to probe the binding of **2b–6b** to the 16-*mer* peptide H-Asp-Ala-Glu-Phe-Arg-His-Asp-Ser-Gly-Tyr-Glu-Val-His-His-Gln-Lys-OH (see ESI† for a description of data analysis, see Table 1 for adducts analysed and location of metallated residues). Analysis of the ETD spectra of the 1 : 1 [peptide + **2b** + 2H − 2Cl]$^{4+}$ and [peptide + **2b** + 2H − 2Cl − PTA]$^{4+}$ adducts revealed complex binding at the His^6, His^{13} and His^{14} sites. These observations could correspond to crosslinking of sites His^6, His^{13} or His^{14} through metallation by a single Ru complex where crosslinking then breaks apart upon ETD fragmentation, or could correspond to a population of three metallated peptides within the sample, where the site of modification is solely at His^6, His^{13} or His^{14}.

For dinuclear complexes **3b–6b**, ETD spectra provided direct evidence that each of the complexes was able to crosslink the peptide through simultaneous coordination of each ruthenium centre to one or more different histidine residues at His^6, His^{13} and His^{14} (Fig. 4). Further peptide adducts of each metal complex were analysed where either a single metallated histidine site was identified or no metallated amino acid sites were clearly identified (although metallation at the terminal amino acid residues was discounted). These spectra provide only a partial picture of the sites of metallation in these adducts but, given the 1 : 1 peptide–complex stoichiometries of the adducts, they also provide evidence towards crosslinking of the peptide through the histidine residues. It was noticeable that ETD spectra with **4b–6b** are very similar for each particular adduct, exhibiting virtually identical fragment distributions in each case (Fig. S21 and S22†). These results suggest that although **4b** and **5b**/**6b** possess different conformations there is sufficient flexibility in these peptide adducts to allow crosslinking through the same histidine positions. To probe these adducts further complementary binding studies were performed using ion mobility-mass spectrometry (IM-MS). IM-MS has been recently used to probe conformational changes in the protein ubiquitin on platination with cisplatin[38] and also in combination with fragmentation techniques to identify drug metallation sites on peptides.[36]

We used IM-MS to probe the different complex–peptide adducts analysed by ETD fragmentation and comparisons of their arrival time distributions (ATDs) have been made (Table 2, Fig. 5, 6 and S23–S26†). For the mononuclear complex-peptide adduct formed through loss of all chlorido and a PTA ligand [peptide + 2b + 2H − 2Cl − PTA]$^{4+}$ a single peak was observed in the ATD indicating this adduct exists as a single isomer in the gas phase. For the equivalent adducts of the dinuclear complexes ([peptide + **X** − 4Cl − PTA]$^{4+}$ (**X** = **3b–6b**)) the ATDs are more complex and exhibit two peaks (Fig. 5) indicating these adducts all exist as two isomeric species in the gas phase. For 1 : 1 peptide–complex adducts, formed through loss of all chlorido ligands from Ru whilst retaining all their PTA ligands ([peptide + **X** + nH − nCl]$^{4+}$ (**X** = **2b–6b**)), the ATDs in each case consist of two peaks. These results show each adduct in this series also exists as two isomeric species in the gas phase. A comparison of the drift times at which each peak in the ATDs is centred revealed that peaks for the [peptide + **X** + nH − nCl]$^{4+}$ adducts are all centred at equal or longer drift times than their corresponding [peptide + **X** + nH − nCl − PTA]$^{4+}$ adducts (**X** = **2b–6b**). This reflects the larger size of the former adducts due to their retention of the PTA ligand, and highlights the important role played by the ligand set around the Ru ion in determining the shape of the adduct formed. The split distributions observed in the ATDs of all the dinuclear Ru compound–peptide adducts are likely due to crosslinking of the peptide by the dinuclear compounds between His^6–His^{13} and His^6–His^{14} to yield two adducts of different size. In contrast, the single peak observed in the ATD of the adduct [peptide + **2b** + 2H − 2Cl − PTA]$^{4+}$ may be due to the metallation at the three histidine sites, as observed in the ETD analysis, yielding three adducts of identical size. An alternative interpretation is that the peptide is crosslinked by a single metal complex through sites His^6, His^{13} and His^{14} to yield a single adduct; this interpretation correlates with the metal fragment of this adduct having lost two chlorido and one PTA ligand. Similar to the ETD analysis of the peptide adducts of the isomeric complexes **4b–6b** no differences are observed in the ATDs of their peptide adducts, or between the ATDs of the [**X** − 4Cl + 2OH + 2H_2O]$^{2+}$ (**X** = **4b–6b**, Fig. S25†) ions themselves. Combined, these data indicate that despite the different conformations of the three complexes, as confirmed by crystallographic and ^{1}H NMR analysis, they have an identical size, at least in the gas phase. In addition, these data show that adducts formed between the peptide and the metal complexes are similar in terms of their size and in terms of their preferential binding sites.

Table 1 Peptide–complex adducts subjected to electron-transfer dissociation fragmentation and identified sites of metallation

Adduct	Identified site of metallation
[Peptide + **2b** + 2H − 2Cl]$^{4+}$	His^6, His^{13} and His^{14}
[Peptide + **2b** + 2H − 2Cl − PTA]$^{4+}$	His^6, His^{13} and His^{14}
[Peptide + **3b** + H − 4Cl]$^{5+}$	His^6 and His^{13}
[Peptide + **3b** − PTA − 4Cl]$^{4+}$	His^6, other sites unidentified
[Peptide + **3b** − 4Cl]$^{4+}$	His^6, other sites unidentified
[Peptide + **X** + H − 4Cl − PTA]$^{5+}$ (**X** = **4b**, **5b** or **6b**)	His^6 and His^{13} or His^{14}
[Peptide + **X** + H − 4Cl]$^{5+}$ and [peptide + **X** − 4Cl − PTA]$^{4+}$ (**X** = **4b**, **5b** or **6b**)	Central amino acid residues (no metallation observed at terminal residues)

Evaluation of *in vitro* anticancer activity

The cytotoxicity of **2a–6a** and **2b–6b** was assessed in human ovarian carcinoma (A2780), human ovarian carcinoma with acquired resistance to cisplatin (A2780cisR) and human

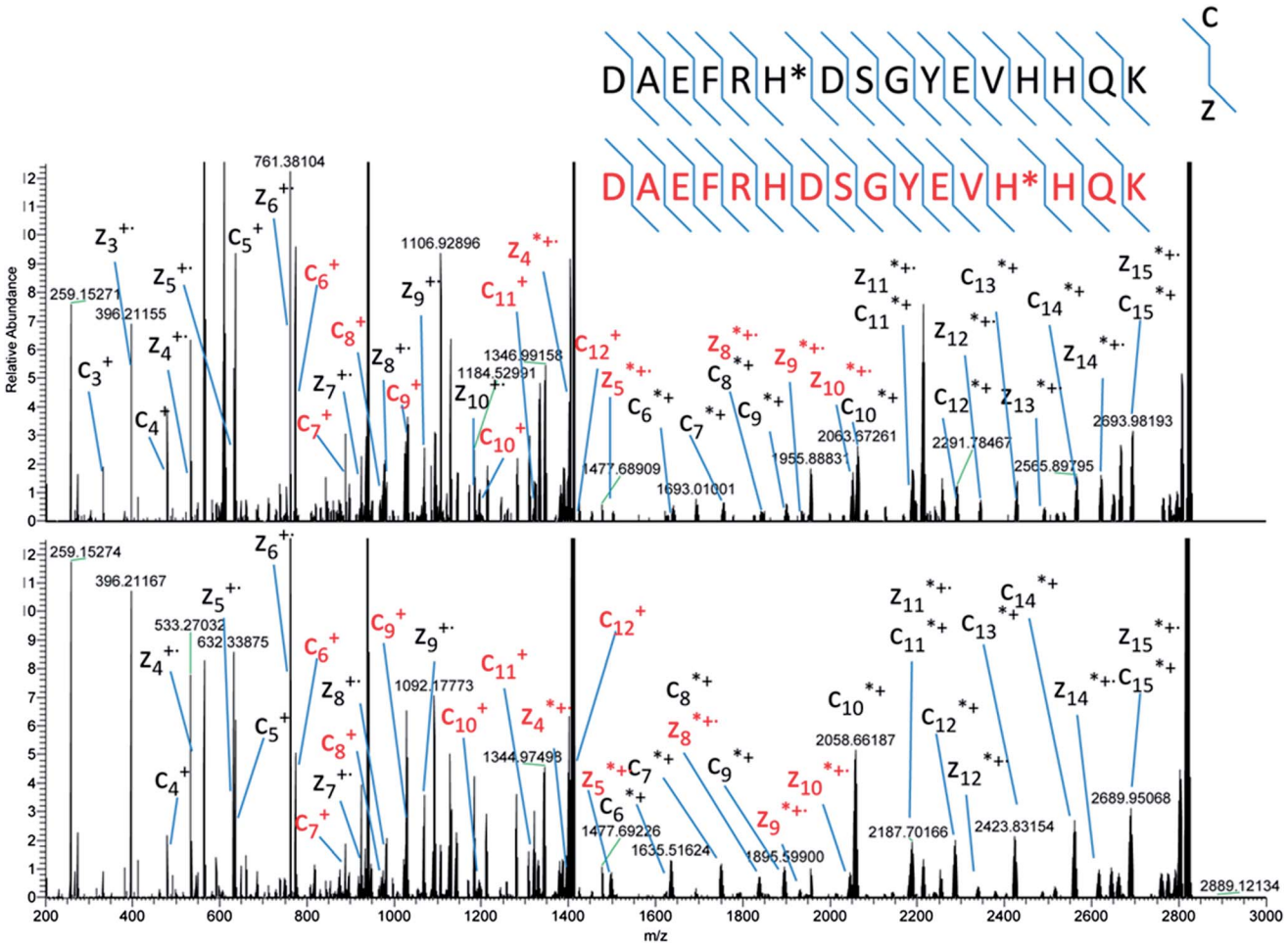

Fig. 4 ETD LTQ Orbitrap FTMS of the [H-Asp-Ala-Glu-Phe-Arg-His-Asp-Ser-Gly-Tyr-Glu-Val-His-His-Gln-Lys-OH + **3b** + H − 4Cl]$^{5+}$ adduct (top) and the [H-Asp-Ala-Glu-Phe-Arg-His-Asp-Ser-Gly-Tyr-Glu-Val-His-His-Gln-Lys-OH + **5b** + H − 4Cl − PTA]$^{5+}$ adduct (bottom) after a 100 ms interaction period with fluoroanthene radical anions. Fragments corresponding to metallation at His^{6} are labelled in black whereas fragments labelled in red are those corresponding to metallation at His^{13}. Fragments labelled with * correspond to a metallated fragment.

Table 2 Data from IM-MS studies showing ion mobility drift times of peak maxima, measured monoisotopic masses of selected peptide adducts or complex ions and the corresponding theoretical values

Peptide adduct/ion	Ion mobility drift time(s) (ms)	Measured monoisotopic mass (m/z)	Theoretical monoisotopic mass (m/z)
[Peptide + **2b** + 2H − 2Cl − PTA]$^{4+}$ ($C_{97}H_{140}N_{28}O_{29}Ru$)	2.93	565.77	565.73
[Peptide + **3b** − 4Cl − PTA]$^{4+}$ ($C_{112}H_{159}N_{32}O_{30}PRu_2$)	2.88, 3.15	666.78	666.74
[Peptide + **4b** − 4Cl − PTA]$^{4+}$ ($C_{124}H_{167}N_{32}O_{30}PRu_2$)	2.98, 3.42	704.80	704.76
[Peptide + **5b** − 4Cl − PTA]$^{4+}$ ($C_{124}H_{167}N_{32}O_{30}PRu_2$)	2.98, 3.42	704.80	704.76
[Peptide + **6b** − 4Cl − PTA]$^{4+}$ ($C_{124}H_{167}N_{32}O_{30}PRu_2$)	2.98, 3.42	704.80	704.76
[Peptide + **2b** + 2H − 2Cl]$^{4+}$ ($C_{103}H_{152}N_{31}O_{29}PRu$)	2.98, 3.09	605.04	605.00
[Peptide + **3b** − 4Cl]$^{4+}$ ($C_{118}H_{171}N_{35}O_{30}P_2Ru_2$)	2.93, 3.42	706.06	706.01
[Peptide + **4b** − 4Cl]$^{4+}$ ($C_{130}H_{179}N_{35}O_{30}P_2Ru_2$)	3.04, 3.53	744.07	744.03
[Peptide + **5b** − 4Cl]$^{4+}$ ($C_{130}H_{179}N_{35}O_{30}P_2Ru_2$)	2.98, 3.53	744.08	744.03
[Peptide + **6b** − 4Cl]$^{4+}$ ($C_{130}H_{179}N_{35}O_{30}P_2Ru_2$)	2.98, 3.58	744.07	744.03
[**4b** + 2OH + 2H_2O − 4Cl]$^{2+}$ ($C_{46}H_{66}N_8O_6P_2Ru_2$)	2.66, 2.88	546.12	546.13
[**5b** + 2OH + 2H_2O − 4Cl]$^{2+}$ ($C_{46}H_{66}N_8O_6P_2Ru_2$)	2.66, 2.88	546.12	546.13
[**6b** + 2OH + 2H_2O − 4Cl]$^{2+}$ ($C_{46}H_{66}N_8O_6P_2Ru_2$)	2.66, 2.88	546.12	546.13
[Peptide + 4H]$^{4+}$ ($C_{84}H_{123}N_{27}O_{28}$)	2.66	489.51	489.48

embryonic kidney (HEK 293) cell lines using the MTT assay (Table 3). As discussed earlier, the cytotoxicity of the original RAPTA series toward a range of cancer cell lines is low (IC_{50} often >300 μM) and these high IC_{50} values are mirrored by the values determined for mononuclear compounds **2a** and **2b**, which are >300 μM in the three cell lines. All dinuclear

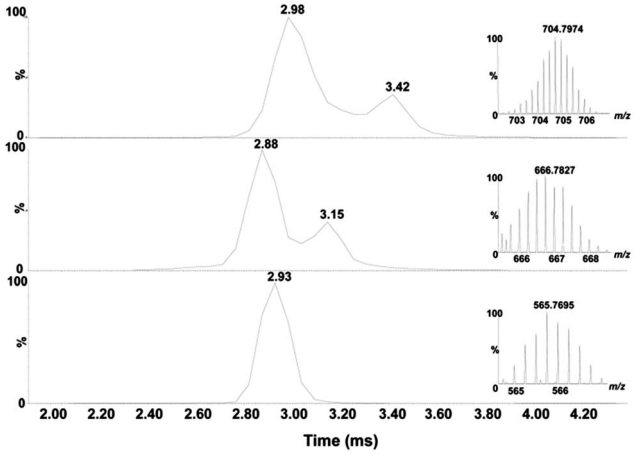

Fig. 5 Comparison of the ATDs of the [peptide + **2b** − 2Cl − PTA + 2H]$^{4+}$ (bottom), [peptide + **3b** − 4Cl − PTA]$^{4+}$ (middle) and [peptide + **4b** − 4Cl − PTA]$^{4+}$ (top) adducts. Inset shows the isotope profile of the corresponding mass peaks in the mass spectrum.

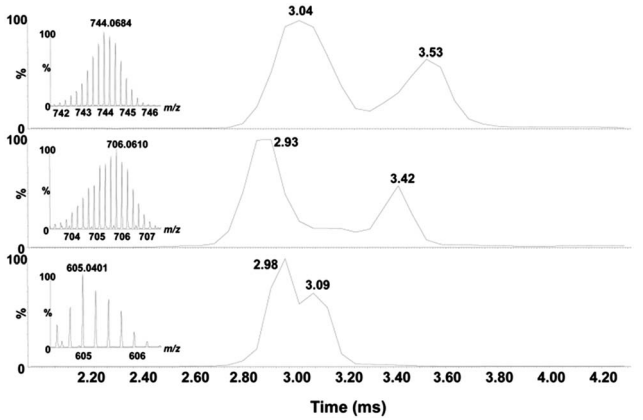

Fig. 6 Comparison of the ATDs of the [peptide + **2b** − 2Cl + 2H]$^{4+}$ (bottom), [peptide + **3b** − 4Cl]$^{4+}$ (middle) and [peptide + **4b** − 4Cl]$^{4+}$ (top) adducts. Inset shows the isotope profile of the corresponding mass peaks in the mass spectrum.

compounds **3a–6a** and **3b–6b** are significantly more cytotoxic against the A2780 cell line than the mononuclear analogues. Of these, the most cytotoxic compounds are those with the closed conformation, *i.e.* **5a**, **6a**, **5b** and **6b**, with the chlorido-analogues (**5b** and **6b**) being slightly more cytotoxic than the oxalato-analogues (**5a** and **6a**). Interestingly, the diastereoisomeric complexes **4a** and **4b** are significantly less active, with IC_{50} values increasing over 5-fold in the case of the chlorido-analogue and over 2-fold for the oxalato-analogue. The flexible dinuclear oxalato-complex, **3a**, has a comparable cytotoxicity to that of **4a** whereas the IC_{50} value of the chlorido analogue, **3b**, is significantly greater than that of **4b**.

In the A2780cisR cell line the IC_{50} values of complexes **5a**, **6a**, **5b** and **6b** remain low, albeit, for complexes **6a** and **6b**, with the linker of (*R*,*R*)-configuration, with a slight increase in IC_{50} values relative to those values obtained for the A2780 cell line. The IC_{50} values of complexes **5a** and **5b**, with the linker of (*S*,*S*)-configuration, remain essentially unchanged. In contrast, the IC_{50} values for **3a** and **3b** (linked by the flexible ethylenediamine moiety) and **4a** and **4b** (with the linker of (*R*,*S*)-configuration) increase dramatically. For example, **4a** and **4b** possess IC_{50} values 7 and 21 times, respectively, greater than those of their most active diastereoisomers (**5a** and **5b**) whereas **3a** is 9 fold less cytotoxic than the most active oxalato-compound **5a**, and **3b** is essentially inactive in the A2780cisR cell line (IC_{50} > 300 μM). In addition, compounds **5b** and **6b** are significantly more active than cisplatin in this cell line (over 3 fold in the case of **5b**).

In the HEK-293 cell line, used as a model for non-tumorigenic cells, the activity of the compounds follows the pattern of activity of the compounds observed in the A2780 cell line. The cytotoxicity of **5a**, **6a**, **5b** and **6b** towards this cell line remains higher than that of **3a**, **3b**, **4a** and **4b** with no significant differences in IC_{50} values between chlorido- and oxalato-analogues observed for each case. One exception is that in this cell line the activity of the chlorido complex **3b** is greater than that observed in the A2780 and A2780cisR cell lines and comparable to the value of its oxolato analogue **3a**, which in other cell lines is more active.

The differences in activity between diastereoisomeric complexes **4a–6a** and **4b–6b** are significant, with an apparent conformational dependence observed for both cytotoxic activity and also for susceptibility to resistance in the A2780cisR cell line. The complexes with the "closed" conformation consistently show high cytotoxicity against all cell lines examined, and in the case of **5a** and **5b**, with the linker of (*S*,*S*)-configuration, virtually no loss of activity against the A2780cisR cell line. In contrast, the compounds with the more open structure (**4a** and **4b** incorporating the linker of (*R*,*S*)-configuration), or those with a flexible ethylenediamine linker that may also be expected to occupy an open conformation (**3a** and **3b**), are significantly less cytotoxic and also show a dramatic decrease in cytotoxicity against the A2780cisR cell line. To probe whether the origin of these observations were due to the differential intracellular uptake of these complexes, A2780 cells were incubated for 5 h with **2a–6a** (300 μM) and the intracellular ruthenium content was determined using ICP-MS. It was found that the level of internalised **4a** (391 ± 52 pmol Ru per 10^6 cells) is comparable to that observed for **5a** (332 ± 25 pmol Ru per 10^6 cells). Unexpectedly, under identical incubation conditions the level of **6a** (901 ± 97 pmol Ru per 10^6 cells) is significantly higher than that observed for **5a** despite it having a very similar cytotoxicity profile. At present, the origins of this differential uptake are unknown, though a recent report has shown the chirality of substituents on the ruthenium arene ligand can have a significant influence on biological activity.[39] Compound **3a** exhibits slightly higher cellular uptake levels (474 ± 21 pmol Ru per 10^6 cells) than **4a** and **5a** whereas the mononuclear analogue **2a** (459 ± 89 pmol Ru per 10^6 cells) displays the highest level of internalised complex of all the compounds. These results indicate that while the levels of ruthenium cellular uptake do not correlate with the cytotoxicity profiles of the compounds at 72 h, all compounds, under the experimental conditions, readily internalise in A2780 cells and at comparable levels observed for RAPTA-T.[19] In addition to these uptake studies

Table 3 *In vitro* anticancer activity of compounds **2a–6b** in human ovarian carcinoma (A2780), human ovarian carcinoma cisplatin resistant (A2780cisR) and human embryonic kidney 293 (HEK-293) cell lines after 72 h exposure, octanol–water partition coefficients for compounds **2a–6a** and cellular (A2780) uptake of ruthenium after exposure to **2a–6a** for 5 h exposure at 300 μM

	IC_{50} (μM)				
Compound	A2780	A2780cisR	HEK-293	log *P*	Cellular uptake (pmol ruthenium per 10^6 cells)
2a	>400	>400	>400	−1.57	459 ± 89
3a	23 ± 0.5	88 ± 10	29 ± 2.5	−1.26	474 ± 21
4a	25 ± 2.5	74 ± 6	19 ± 4	−1.38	391 ± 52
5a	10 ± 0.5	10 ± 1	6 ± 1	−1.41	332 ± 25
6a	8.5 ± 0.5	15 ± 0.5	6 ± 0.5	−1.36	901 ± 97
2b	>300	>300	>300	—	—
3b	64 ± 9.5	>300	35 ± 3	—	—
4b	20 ± 0.5	95 ± 6.5	24 ± 3.5	—	—
5b	3.7 ± 0.6	4.5 ± 0.2	8 ± 0.5	—	—
6b	3.7 ± 0.6	7.0 ± 0.5	5.9 ± 0.2	—	—
Cisplatin	1.5 ± 0.2	14.5 ± 2	7.5 ± 1	—	—

the log *P* values for complexes **2a**, **3a**, **4a**, **5a** and **6a** were determined using the shake-flask method.[40] These experiments reveal the hydrophilic nature of all complexes with little variation in log *P* within the series. Therefore it is reasonable to conclude that the differences in the cytotoxicity, at least in the A2780 cell line, must be due to cellular events associated with the complexes and their ability to crosslink target biomolecules as demonstrated in binding studies, and is not due to significant differences in complex hydrophilicity and cellular uptake.

Conclusions

We have developed a new route to arene-functionalised organometallic Ru(II) compounds, allowing access to flexible and conformationally rigid dinuclear organometallic Ru(II) complexes. Crystallographic studies and NMR spectroscopy revealed that the stereochemical configuration of the 1,2-diphenylethylenediamine (DPEN) linker controls whether the dinuclear complexes have an open or closed conformation. The range of adducts formed between these rigid dinuclear complexes, **4b–6b** and the small molecules 5′-GMP and L-histidine appears to be governed by the conformation of the complex, and all dinuclear complexes **3b–6b** are capable of crosslinking model peptide/oligonucleotide sequences. The mononuclear complexes, as observed for the original RAPTA series, are non-cytotoxic whereas dinuclear complexes are significantly more cytotoxic. Although the different conformations of **4b** *vs.* **5b**/**6b** resulted in no differences in type and size of adducts formed in model peptide binding studies, an apparent conformational dependence on the cytotoxicity of these dinuclear complexes was observed. Those with the more closed conformation (**5a–6b**) are significantly more cytotoxic than those with the more open conformation (**4a** and **4b**) and are unaffected by resistance mechanisms operating in the A2780cisR cell line. In contrast, **4a** and **4b** were significantly less cytotoxic toward this cell line than the A2780 cell line. However, for all dinuclear complexes, cytotoxicity toward the cancerous A2780 cell line and the non-cancerous HEK-293 cell line varied little. Further studies revealed the hydrophilicity of the compounds, as assessed by measurement of log *P* values, was similar within the series **2a–6a**, and uptake experiments with A2780 cells revealed an appreciable level of complex association in each case. Combined, these observations lead to the conclusions that the different cytotoxicities of the mononuclear and dinuclear compounds is linked to the ability of the complex to crosslink biomolecular targets and that the cytotoxicity of the dinuclear compounds is significantly linked to their conformation.

Acknowledgements

This work was supported by a Marie Curie Intra-European Fellowship within the 7th European Community Framework Programme (Project 273658-DINURU to B.S.M). We thank the Nestle Institute of Health Sciences for access to the Synapt G2-S quadrupole-time-of-flight HDMS mass spectrometer and Julien Bourquin for assistance in data collection and analysis. We thank Dr Luc Patiny for developing calculation tools for interpretation of ETD fragmentation spectra. We thank Baihua Ye for chiral HPLC analysis and Prof. Nicolai Cramer for access to these facilities.

Notes and references

‡ Structural data obtained from single crystals of samples of **5a** and **6a** is identical, with each crystal found to contain a 50 : 50 mixture of **5a** and **6a** resulting in the solved structures exhibiting disorder in the region of the chiral centres of the DPEN linker molecule. As the (1*S*,2*S*)-DPEN and (1*R*,2*R*)-DPEN linkers utilised in the synthesis of **5a** and **6a** respectively were commercial samples with a stated enantiomeric excess of 98% and 99% respectively, we postulate the racemic composition of crystals of **5a** and **6a** are not reflective of the bulk sample, but are most likely a result of the co-crystallization of the desired and undesired enantiomers present in the samples. Chiral HPLC was used to determine the percentage of each enantiomer in bulk samples of **5a** and **6a** by analysis of the arene ligand following cleavage from the Ru ions (see Experimental section and Fig. S2–S4† for details). This analysis showed that **5a** was obtained with an enantiomeric excess of 99.4% and **6a** was obtained with an enantiomeric excess of

99.8%. These results confirm that the bulk samples of **5a** and **6a** are of a high level of enantiomeric purity and indicate that co-crystallization of the enantiomeric impurity in each sample with the bulk product is the source of the racemic crystals obtained.

1 X. Wang and Z. Guo, *Chem. Soc. Rev.*, 2013, **42**, 202.
2 A. K. Singh, D. S. Pandey, Q. Xu and P. Braunstein, *Coord. Chem. Rev.*, 2013, DOI: 10.1016/j.ccr.2013.09.009.
3 A. Habtemariam, M. Melchart, R. Fernández, S. Parsons, I. D. H. Oswald, A. Parkin, F. P. A. Fabbiani, J. E. Davidson, A. Dawson, R. E. Aird, D. I. Jodrell and P. J. Sadler, *J. Med. Chem.*, 2006, **49**, 6858.
4 W. F. Schmid, R. O. John, V. B. Arion, M. A. Jakupec and B. K. Keppler, *Organometallics*, 2007, **26**, 6643.
5 A. Kurzwernhart, W. Kandioller, É. A. Enyedy, M. Novak, M. A. Jakupec, B. K. Keppler and C. G. Hartinger, *Dalton Trans.*, 2013, **42**, 6193.
6 S. M. Meier, M. Hanif, Z. Adhireksan, V. Pichler, M. Novak, E. Jirkovsky, M. A. Jakupec, V. B. Arion, C. A. Davey, B. K. Keppler and C. G. Hartinger, *Chem. Sci.*, 2013, **4**, 1837.
7 E. Meggers, G. E. Atilla-Gokcumen, K. Gründler, C. Frias and A. Prokop, *Dalton Trans.*, 2009, **48**, 10882.
8 N. P. E. Barry, O. Zava, J. Furrer, P. J. Dyson and B. Therrien, *Dalton Trans.*, 2010, **39**, 5272.
9 N. P. E. Barry, F. Edafe and B. Therrien, *Dalton Trans.*, 2011, **40**, 7172.
10 A. Dubey, J. W. Min, H. J. Koo, H. Kim, T. R. Cook, S. C. Kang, P. J. Stang and K.-W. Chi, *Chem. – Eur. J.*, 2013, **19**, 11622.
11 H. Jung, A. Dubey, H. J. Koo, V. Vajpayee, T. R. Cook, H. Kim, S. C. Kang, P. J. Stang and K.-W. Chi, *Chem. – Eur. J.*, 2013, **19**, 6709.
12 V. Vajpayee, S. Lee, J. W. Park, A. Dubey, H. Kim, T. R. Cook, P. J. Stang and K.-W. Chi, *Organometallics*, 2013, **32**, 1563.
13 V. Vajpayee, Y. J. Yang, S. C. Kang, H. Kim, I. S. Kim, M. Wang, P. J. Stang and K.-W. Chi, *Chem. Commun.*, 2011, **47**, 5184.
14 N. P. E. Barry, O. Zava, P. J. Dyson and B. Therrien, *Chem. – Eur. J.*, 2011, **17**, 9669.
15 M. A. Furrer, A. Garci, E. Denoyelle-Di-Muro, P. Trouillas, F. Giannini, J. Furrer, C. M. Clavel, P. J. Dyson, G. Süss-Fink and B. Therrien, *Chem. – Eur. J.*, 2013, **19**, 3198.
16 P. Govender, A. K. Renfrew, C. M. Clavel, P. J. Dyson, B. Therrien and G. S. Smith, *Dalton Trans.*, 2011, **40**, 1158.
17 C. Scolaro, A. Bergamo, L. Brescacin, R. Delfino, M. Cocchietto, G. Laurenczy, T. J. Geldbach, G. Sava and P. J. Dyson, *J. Med. Chem.*, 2005, **48**, 4161.
18 A. Bergamo, A. Masi, P. J. Dyson and G. Sava, *Int. J. Oncol.*, 2008, **33**, 1281.
19 D. A. Wolters, M. Stefanopoulou, P. J. Dyson and M. Groessl, *Metallomics*, 2012, **4**, 1185.
20 B. Wu, M. S. Ong, M. Groessl, Z. Adhireksan, C. G. Hartinger, P. J. Dyson and C. A. Davey, *Chem. – Eur. J.*, 2011, **17**, 3562.
21 A. Casini, C. Gabbiani, E. Michelucci, G. Pieraccini, G. Moneti, P. J. Dyson and L. Messori, *J. Biol. Inorg. Chem.*, 2009, **14**, 761.
22 A. Casini, C. Gabbiani, F. Sorrentino, M. Pia Rigobello, A. Bindoli, T. J. Geldbach, A. Marrone, N. Re, C. G. Hartinger, P. J. Dyson and L. Messori, *J. Med. Chem.*, 2008, **51**, 6773.
23 W. H. Ang, L. J. Parker, A. De Luca, L. Juillerat-Jeanneret, C. J. Morton, M. Lo Bello, M. W. Parker and P. J. Dyson, *Angew. Chem., Int. Ed.*, 2009, **48**, 3854.
24 R. A. Ruhayel, J. S. Langner, M.-J. Oke, S. J. Berners-Price, I. Zgani and N. P. Farrell, *J. Am. Chem. Soc.*, 2012, **134**, 7135.
25 C. Billecke, S. Finniss, L. Tahash, C. Miller, T. Mikkelsen, N. P. Farrell and O. Bögler, *Neurooncology*, 2006, **8**, 215.
26 L. Gatti, P. Perego, R. Leone, P. Apostoli, N. Carenini, E. Corna, C. Allievi, U. Bastrup, S. De Munari, S. Di Giovine, P. Nicoli, M. Grugni, M. Natangelo, G. Pardi, G. Pezzoni, J. W. Singer and F. Zunino, *Mol. Pharmaceutics*, 2010, **7**, 207.
27 C. G. Hartinger, A. D. Phillips and A. A. Nazarov, *Curr. Top. Med. Chem.*, 2011, **11**, 2688.
28 M. G. Mendoza-Ferri, C. G. Hartinger, R. E. Eichinger, N. Stolyarova, K. Severin, M. A. Jakupec, A. A. Nazarov and B. K. Keppler, *Organometallics*, 2008, **27**, 2405.
29 M. G. Mendoza-Ferri, C. G. Hartinger, M. A. Mendoza, M. Groessl, A. E. Egger, R. E. Eichinger, J. B. Mangrum, N. P. Farrell, M. Maruszak, P. J. Bednarski, F. Klein, M. A. Jakupec, A. A. Nazarov, K. Severin and B. K. Keppler, *J. Med. Chem.*, 2009, **52**, 916.
30 O. Nováková, A. A. Nazarov, C. G. Hartinger, B. K. Keppler and V. Brabec, *Biochem. Pharmacol.*, 2009, **77**, 364.
31 A. M. Pizarro, A. Habtemariam and P. J. Sadler, *Top. Organomet. Chem.*, 2010, **32**, 21.
32 M. Groessl, Y. O. Tsybin, C. G. Hartinger, B. K. Keppler and P. J. Dyson, *J. Biol. Chem.*, 2010, **15**, 677.
33 H. Chen, J. A. Parkinson, R. E. Morris and P. J. Sadler, *J. Am. Chem. Soc.*, 2003, **125**, 173.
34 A. Dorcier, P. J. Dyson, C. Gossens, U. Rothlisberger, R. Scopelliti and I. Tavernelli, *Organometallics*, 2005, **24**, 2114.
35 K. O. Zhurov, L. Fornelli, M. D. Wodrich, Ü. A. Laskay and Y. O. Tsybin, *Chem. Soc. Rev.*, 2013, **42**, 5014.
36 J. P. Williams, J. M. Brown, I. Campuzano and P. J. Sadler, *Chem. Commun.*, 2010, **46**, 5458.
37 S. M. Meier, Y. O. Tsybin, P. J. Dyson, B. K. Keppler and C. G. Hartinger, *Anal. Bioanal. Chem.*, 2012, **402**, 2655.
38 J. P. Williams, H. I. A. Phillips, I. Campuzano and P. J. Sadler, *J. Am. Soc. Mass Spectrom.*, 2010, **21**, 1097.
39 K. J. Kilpin, S. M. Cammack, C. M. Clavel and P. J. Dyson, *Dalton Trans.*, 2013, **42**, 2008.
40 J. Sangster, *J. Phys. Chem. Ref. Data*, 1989, **18**, 1111.